Complex Ligand-Induced Conformational Changes in $tRNA^{Asp}$ Revealed by Single-Nucleotide Resolution SHAPE Chemistry†

Bin Wang, Kevin A. Wilkinson, and Kevin M. Weeks*

Department of Chemistry, University of North Carolina, Chapel Hill, North Carolina 27599-3290

Received December 5, 2007; Revised Manuscript Received January 13, 2008

ABSTRACT: RNA conformation is both highly dependent on and sensitive to the presence of charged ligands. Mono- and divalent ions stabilize the native fold of RNA, whereas other polyvalent cationic ligands can act to both stabilize or disrupt native RNA structure. In this work, we analyze the effects of two ligands, Mg^{2+} and tobramycin, on the folding of *S. cerevisiae* $tRNA^{Asp}$ transcripts using single nucleotide resolution SHAPE chemistry. Surprisingly, reducing the Mg^{2+} concentration favors a structural rearrangement in which the D- and variable loops pair. The tobramycin polycation binds to loops in $tRNA^{Asp}$ and induces RNA unfolding in two distinct transitions: the loss of tertiary interactions between the T- and D-loops followed by complete unfolding of the D-stem. Although Mg^{2+} and tobramycin are relatively simple ligands, both modulate $tRNA^{Asp}$ folding in unanticipatedly complex ways, neither of which is consistent with simple hierarchical folding or unfolding of this RNA. Monitoring the structural consequences of ligand binding to RNA at single nucleotide resolution makes it possible to define intermediate structures that contribute to the complex energy landscapes often observed for RNA folding processes and lays the groundwork for a significantly improved understanding of the interactions between RNA and its solution environment.

Almost all RNA strands fold back on themselves to form complex secondary and tertiary structures. Because the RNA backbone is polyanionic, the structures accessible to an RNA are highly dependent on ligands present in the solution environment (Figure 1A) (*1–5*). The magnesium cation (Mg^{2+}) plays the most prominent role in RNA folding for two reasons: (i) it is the most abundant divalent ion in biological systems (*6*) and (ii) it is a small multivalent ion, which results in both a high charge density and affinity for phosphate groups. A single Mg^{2+} ion functions to reduce electrostatic stress at the RNA backbone roughly as well as two monovalent ions, but at a much lower entropic cost because fewer ions need to be confined near the RNA (*7, 8*). The largest effect of Mg^{2+} on RNA structure appears to reflect diffusive binding rather than site-specific interactions (*8, 9*). Mg^{2+} thus competes for its electrostatic interactions with RNA with all ions in the solution.

Because of this competition, additional RNA ligands may bind in place of Mg^{2+} resulting in complex structural consequences. One important class of multivalent RNA ligands in this category are the polycationic aminoglycoside antibiotics (*10*). One of the best studied aminoglycosides, tobramycin (TOB^{5+}, Figure 1A), contains five $-NH_3^+$ groups and binds to helical RNAs over roughly four base pairs using at least three of its charged groups (*11*). In this relatively nonspecific interaction mode, binding by TOB^{5+} and other aminoglycosides generally increases duplex stability. This ability to stabilize duplexes increases proportionally with net antibiotic charge (*11–13*).

Aminoglycosides can also interact with RNA in a second specific or semispecific binding mode. The resulting effects on RNA structure are complex. For example, neomycin B binding reinforces the native tertiary structure of yeast $tRNA^{Phe}$ (*14, 15*). In contrast, the closely related tobramycin antibiotic destabilizes folding of yeast $tRNA^{Asp}$ (*16*). In both cases, antibiotic binding interferes with the function of these tRNAs.

A full understanding of the interplay of forces that govern RNA folding will require not only knowledge of native three-dimensional structures, which can be obtained by high-resolution structure determination methods, but also structural information for the intermediate states that are energetically accessible to the native state. Although intermediate states are widely observed in RNA folding reactions, structural information on these states is sparse, incomplete, and often indirect. Adequate characterization of RNA folding intermediates requires single-nucleotide resolution information for nearly all positions in an RNA because structural arrangements may result in only a few unpaired nucleotides becoming constrained or vice versa. Single nucleotide resolution SHAPE[1] chemistry can provide the information required to discriminate among distinct models for a given RNA state (*17–20*).

SHAPE (selective 2′-hydroxyl acylation analyzed by primer extension) exploits the fact that select electrophiles,

* Corresponding author. E-mail: weeks@unc.edu. Phone: 919-962-7486. Fax: 919-962-2388.

† Supported by a grant from the National Science Foundation (MCB-0416941) to K.M.W.

[1] Abbreviations: SHAPE, selective 2′-hydroxyl acylation analyzed by primer extension; NMIA, *N*-methylisatoic anhydride; 1M7, 1-methyl-7-nitroisatoic anhydride; TOB^{5+}, tobramycin.

10.1021/bi702372x CCC: $40.75
Published on Web 02/22/2008

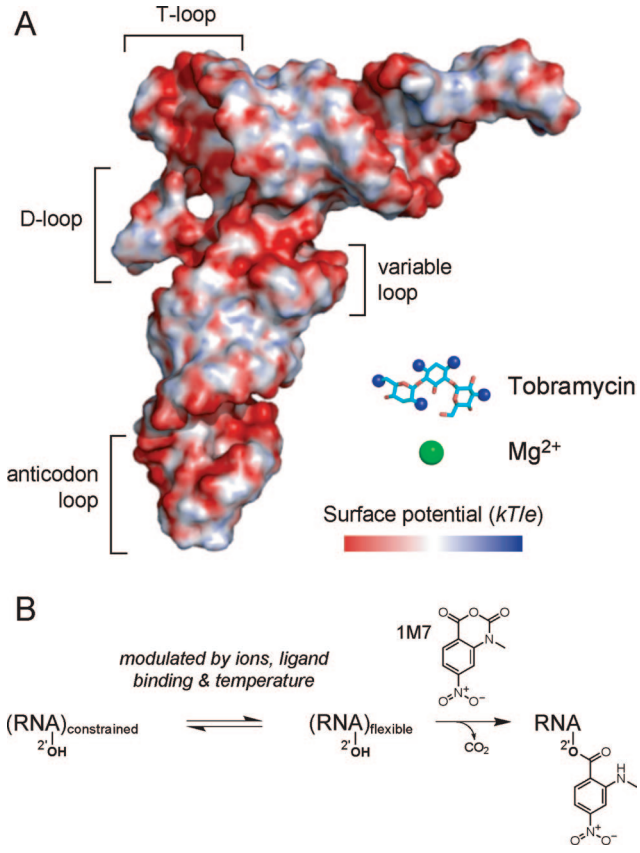

FIGURE 1: (A) Tertiary structure of yeast tRNA^{Asp}, its electrostatic surface potential, and comparison with Mg^{2+} and TOB^{5+} ligands. Surface potential was calculated using the native tRNA^{Asp} structure (*36, 37*) after removing post-transcriptional modifications and using the adaptive Poisson–Boltzmann solver (APBS) with default parameters (*38, 39*). Regions of positive and negative potential are represented in blue and red, respectively; the scale spans ± 40 *kT/e*. (B) Mechanism of RNA SHAPE chemistry and the contributions of ligand binding. Reaction of 2′-hydroxyl groups with 1M7 to form the 2′-*O*-adduct occurs preferentially at flexible nucleotides. Depending on the specific local structural context, ligand binding or other perturbations to an RNA can favor either the constrained state, the flexible state, or have no effect.

including *N*-methylisatoic anhydride (NMIA), react specifically with flexible RNA nucleotides at the ribose 2′-hydroxyl group to form 2′-*O*-adducts (Figure 1B) (*17, 21*). The RNA is modified by NMIA under conditions such that about 1 in 300 nucleotides forms an adduct. Adducts are detected by their ability to stop reverse transcriptase-mediated extension of a 5′-end-labeled DNA primer; termination occurs exactly one nucleotide prior to the modified position. A control extension omitting the reagent to assess background and dideoxy sequencing extensions to match reactive 2′-hydroxyl groups to the sequence are performed in parallel. The resulting cDNAs are then resolved by gel electrophoresis and used to calculate absolute SHAPE reactivity at single nucleotide resolution. With SHAPE, it is typically possible to monitor RNA folding transitions for ≥95% of the positions in an RNA. This level of detail is required to develop credible structural models for well-populated intermediate states.

In one recent analysis, we used SHAPE chemistry to show that tRNA^{Asp} transcripts undergo thermal denaturation by a mechanism involving multistep loss of tertiary structure and a shift in base pairing (*17*). Overall, this analysis of thermally induced unfolding revealed an unanticipatedly complex set of relationships between secondary and tertiary structure that was not consistent with a simple hierarchical model for RNA folding (*17*). This initial work was performed with the SHAPE reagent NMIA, which is well-suited for monitoring temperature-dependent changes in RNA structure (*17*). However, Mg^{2+} modulates the reactivity of NMIA (*22*) and therefore this reagent cannot be used to quantify ion-induced folding of RNA.

Our laboratory has recently introduced a new SHAPE reagent, 1-methyl-7-nitroisatoic anhydride (1M7) (*22*), which has the critical advantage that the intrinsic reactivity of this reagent is not significantly modulated by solution ions, including Mg^{2+} and TOB^{5+}. Therefore, differences in SHAPE reactivity with 1M7 directly reflect RNA structural changes and not ion-induced changes in reagent reactivity (Figure 1B).

In this work, we monitor the structural transitions of tRNA^{Asp} transcripts as a function of Mg^{2+} and TOB^{5+} (Figure 1A). Reducing the concentration of Mg^{2+} and addition of TOB^{5+} both cause tRNA^{Asp} to unfold, but via distinct mechanisms. Removing Mg^{2+} destabilizes tertiary interactions in the variable loop and thereby allows this region to form stable, non-native base pairs with nucleotides in the D-loop. In contrast, addition of tobramycin disrupts the native fold in two distinct transitions, involving loss of tertiary interactions between the T- and D-loops followed by the complete unfolding of the D-stem. Perturbation of tRNA structure by three unfolding methods—temperature, removal of Mg^{2+}, and addition of TOB^{5+}—reveals that each denaturation pathway is unique and involves distinct base pairing and tertiary structure rearrangements. This work also demonstrates that SHAPE chemistry implemented using 1M7 is a highly informative approach for exploring complex RNA folding landscapes as a function of ligand environment.

RESULTS

tRNA^{Asp} Structure. We monitored the structure of in vitro *S. cerevisiae* tRNA^{Asp} transcripts, which lack post-transcriptional modifications. These transcripts both fold into the same three-dimensional structure and show essentially identical enzymatic aminoacylation activity as the native tRNA (*16, 23, 24*). The tRNA transcript was refolded under conditions that stabilize the native conformation of this RNA (6 mM Mg^{2+}, 100 mM NaCl, pH 8) and then treated with 1M7 (Figure 1B). Sites of 2′-*O*-adduct formation were detected by primer extension and comparison with a similar reaction in which 1M7 was omitted (compare "native" lanes in the + and − 1M7 lanes, Figure 2A). Absolute SHAPE reactivities, after subtracting background, were normalized such that 0 indicates no SHAPE reactivity and 1.0 is the average intensity of highly reactive positions. Independent experimental measurements at a given nucleotide are typically reproducible to ±0.05 SHAPE units (see error bars, Figure 2B).

As expected, SHAPE reactivity exactly recapitulates the native structure of tRNA^{Asp}. Nucleotides in the anticodon loop have high SHAPE reactivities (≥0.7), whereas nucleotides in the D- and T-loops are reactive but less so, consistent with involvement in partially constraining tertiary interactions (Figure 2B). Nucleotides that are constrained by base pairing are unreactive. We use these data as a reference to develop single-nucleotide resolution unfolding pathways

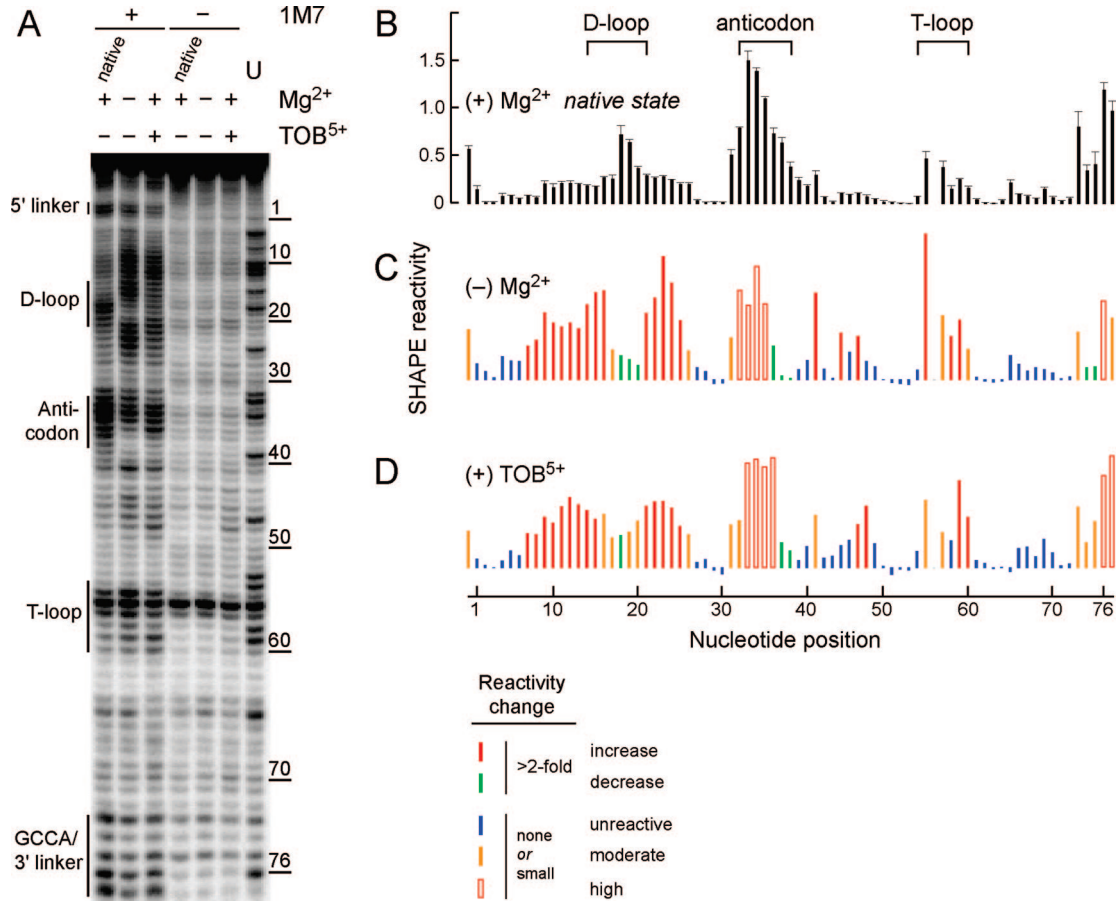

FIGURE 2: SHAPE analysis of yeast $tRNA^{Asp}$ under three reference conditions: in the native state, in the absence of Mg^{2+}, and in the presence of the aminoglycoside antibiotic tobramycin. (A) SHAPE reactivities mapped by primer extension and resolved by denaturing electrophoresis. Reactions were performed as a function of $MgCl_2$ (6 mM) and TOB^{5+} (4.5 mM) in the presence or absence of 1M7. The dideoxy sequencing ladder (U) lane is one nucleotide longer than the corresponding (+) and (−) 1M7 bands. RNA structural landmarks and nucleotide positions refer to the 1M7 lanes. SHAPE reactivities for (B) the native $tRNA^{Asp}$, (C) in the absence of Mg^{2+}, and (D) in the presence of TOB^{5+}. For experiments performed in the absence of Mg^{2+} or in the presence of tobramycin (panels C and D), nucleotides exhibiting 2-fold or larger changes in reactivity as compared to the native state are colored red (increase) and green (decrease), respectively; nucleotides showing <2-fold changes are colored in blue (unreactive, SHAPE reactivity ≤0.3), orange (moderately reactive, 0.3 < SHAPE reactivity < 0.7), and red outline (highly reactive, SHAPE reactivity ≥0.7), respectively. This coloring scheme is used consistently in Figures 3 and 4.

for $tRNA^{Asp}$ as (i) Mg^{2+} is removed and (ii) TOB^{5+} is added to the RNA solution.

Local Nucleotide Flexibility for $tRNA^{Asp}$ in the Absence of Mg^{2+}. When an otherwise identical SHAPE experiment is performed on the tRNA in the absence of Mg^{2+}, we observed multiple reactivity changes throughout the RNA (compare + and − Mg^{2+} lanes, Figure 2A). We will focus on those changes that are 2-fold or greater. By this relatively stringent criterion, there are 29 significant changes located primarily in the D-loop, anticodon loop, and T loop of $tRNA^{Asp}$ (red and green bars, Figure 2C).

SHAPE reactivities at three nucleotides in the D-loop (positions 18–20) decrease, while adjacent nucleotides in the D-stem and loop show significant increases (Figure 2C). Additionally, the reactivities of three nucleotides in the anticodon loop (positions 36–38) decrease significantly, whereas the reactivity of a nearby nucleotide at position 41 increases. Finally, the reactivities of nucleotides in the T-loop (positions 55, 58–59) show a significant increase. Thus, removal of Mg^{2+} induces large-scale changes in the structure of $tRNA^{Asp}$ such that individual nucleotides may experience both large increases and large decreases in local flexibility as judged by the SHAPE experiment (Figure 2C). In order to understand the mechanisms that govern how these transitions occur, we explored Mg^{2+}-dependent structural changes over a wide range of ion concentrations.

Mg^{2+}-Induced Transitions in $tRNA^{Asp}$. As the Mg^{2+} concentration was decreased from 20 to 0 mM (Figure 3A, left-most 19 lanes), we observed smooth transitions for almost every nucleotide in $tRNA^{Asp}$, which could be classified into five groups. In the first group, 8 positions, including 3 nucleotides located in the D-loop and 3 nucleotides located in the anticodon loop, undergo large decreases in their SHAPE reactivities (in green; panels B and C in Figure 3).

In the second group, 21 nucleotides, including all residues in the D-stem and most nucleotides in the D- and T-loops, undergo well-behaved transitions in which their SHAPE reactivities increase smoothly with decreasing Mg^{2+} concentrations (in red; panels B and C in Figure 3). Increased local nucleotide flexibility at these positions is consistent with a general unfolding reaction that involves most regions in the RNA.

For nucleotides in the final three groups, SHAPE reactivities remain roughly constant throughout the Mg^{2+} titration. In the third group, 6 nucleotides (G17, G26, C31, A57, U60, and G73) remain moderately reactive and have SHAPE

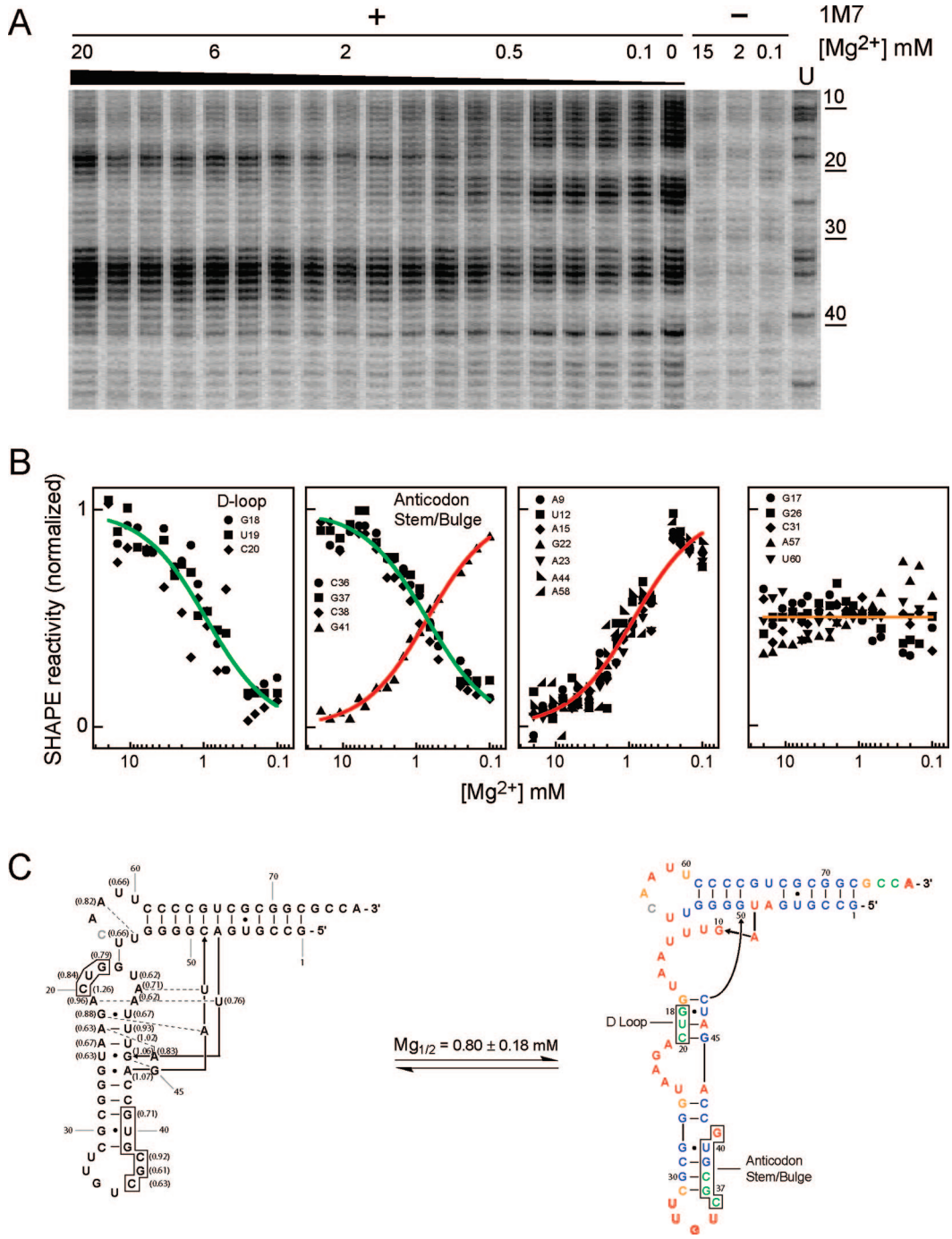

FIGURE 3: Mg^{2+}-dependent unfolding of tRNA^{Asp}. (A) tRNA^{Asp} modification upon removing Mg^{2+} as visualized by RNA SHAPE chemistry. Experiments were performed as a function of [$MgCl_2$] in the presence (+) and absence (−) of reagent. (B) Mg^{2+}-induced structural transitions, illustrated for instructive nucleotide positions. (C) Structural model for unfolding of tRNA^{Asp} in the absence of Mg^{2+}. $Mg_{1/2}$ values are listed for nucleotides that show greater than a 2-fold reactivity change over the titration. Nucleotide coloring system is the same as shown in the legend to Figure 2.

reactivities that do not change by more than ~30% (in orange; panels B and C in Figure 3). In the fourth group, five single-stranded positions located in the anticodon loop and at the 3′-end of tRNA^{Asp} exhibit a uniform high reactivity (SHAPE reactivities ≥0.7, in red outline, Figure 3). Finally, 34 positions, including most residues in the acceptor stem, all residues in the T-stem, part of the anticodon stem, two nucleotides in the variable loop, and U54 in the T-loop, remain unreactive over the entire Mg^{2+} range (in blue; Figure 3C). Observation of a constant low reactivity at these positions indicates that these residues remain stably base paired throughout the transition.

Model for the Rearrangement of tRNA^{Asp} in the Absence of Mg^{2+}. Two additional pieces of information allow us to develop a well-defined model for the final non-native state. First, for all positions showing large increases or decreases in reactivity, we determined the Mg^{2+} concentration at the transition midpoint. The Mg^{2+} concentration midpoints for all transitions are identical at 0.80 ± 0.18 mM (listed in the left-hand panel of Figure 3C). These data are consistent with

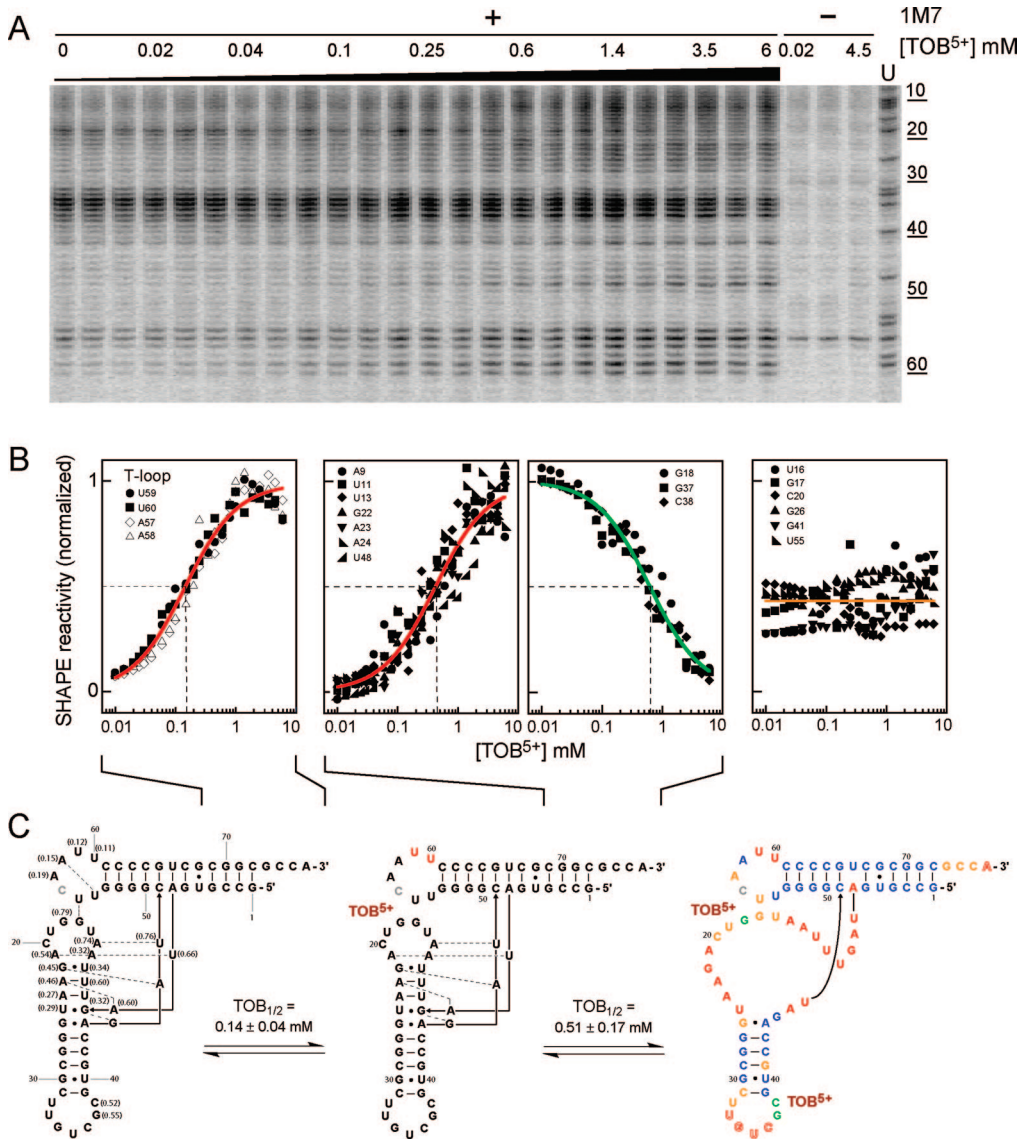

FIGURE 4: Tobramycin-induced unfolding of $tRNA^{Asp}$. (A) Visualization of TOB^{5+}-induced unfolding of $tRNA^{Asp}$. (B) Unfolding transitions for individual positions; transition midpoints are emphasized by dashed lines. (C) Two-step model for TOB^{5+}-induced tRNA unfolding. $TOB_{1/2}$ values are listed for nucleotides that show greater than a 2-fold reactivity change. Nucleotides are colored using the scheme outlined in Figure 2.

a model in which the entire tRNA unfolds in a single, well-defined, transition. Second, during this single transition, most nucleotides become more reactive, but a few in the D-loop and anticodon loop become less reactive (Figure 3B, first two panels). We infer that loss of Mg^{2+} is accompanied by a conformational change that causes these regions to form new, constraining interactions that are not present in the high Mg^{2+} state. Together, these data indicate that removal of Mg^{2+} causes $tRNA^{Asp}$ transcripts to rearrange in a single transition to form an extended, but still highly base paired, structure (Figure 3C, right panel).

This structure readily explains the observed decrease in SHAPE reactivity in the D-loop and anticodon stem and loop regions (emphasized with boxes, Figure 3C). Nucleotides originally in the D-loop (positions 18–20) form new base pairs with positions 45–49 (see boxed nucleotides, Figure 3C). Nucleotides 45–49 are unreactive in the starting state because these nucleotides are constrained by tertiary interactions. These nucleotides remain unreactive in the low Mg^{2+} state because they form new base pairing interactions with nucleotides in the D-loop.

The complex single nucleotide behaviors observed in the anticodon stem region are also consistent with a single conformational change. In this local conformational change, the nucleotides near the anticodon loop rearrange such that G37 and C38, originally located in the anticodon loop, become base-paired to C31 and G30 in the anticodon stem, respectively. Simultaneously, G41 protrudes to from a bulge (boxed nucleotides, Figure 3C). Because of the reduced size of the anticodon loop, the SHAPE reactivity of C36 also decreases. Thus, removal of Mg^{2+} does not cause a simple destabilization of the tertiary structure of this RNA but induces a large scale rearrangement of the D- and anticodon stems.

Tobramycin-Induced Unfolding of $tRNA^{Asp}$. Addition of TOB^{5+} also destabilizes the native tertiary structure of $tRNA^{Asp}$ to yield a final structure that is clearly different from that formed in the absence of Mg^{2+} (compare $-Mg^{2+}$

and +TOB^{5+} lanes in Figure 2A). Eighteen positions, located primarily in the D-stem and loop and the variable loop, experience a 2-fold or greater increase in their SHAPE reactivities at 4.5 mM tobramycin concentration (in red, Figure 2D). In addition, three nucleotides, including one nucleotide in the D-loop (G18) and two nucleotides in the anticodon loop (G37 and C38), experience significant decreases in their reactivities (in green; Figure 2D). The (+) TOB^{5+} state has much less overall structure than both the native and (−) Mg^{2+} states (compare panel D with panels B and C in Figure 2).

Two Transitions for the Unfolding of tRNA^{Asp} by Tobramycin. We evaluated the mechanism of TOB^{5+}-induced unfolding of tRNA^{Asp} by titrating the antibiotic from 0 to 6 mM in the presence of 6 mM Mg^{2+} (24 left-hand lanes, Figure 4A). As was the case with the Mg^{2+} titration, reactivities of the majority of nucleotides remain unchanged upon addition of tobramycin. Thirteen nucleotides in tRNA^{Asp} remain moderately reactive at all tobramycin concentrations (see fourth panel in Figure 4B); U33, G34, U35, C36, and A76 maintain a uniform high reactivity, whereas 35 positions, including most residues in the acceptor stem, all residues in the T-stem, part of the anticodon stem, and select nucleotides in the variable and T-loops, remain unreactive. These data suggest that the acceptor, anticodon, and T-stems remain largely intact in the presence of TOB^{5+} (see third panel, Figure 4C).

We also observed multiple, smooth transitions in the RNA. Twenty-one nucleotides in tRNA^{Asp} undergo reactivity changes of 2-fold or greater during the TOB^{5+} titration (red and green nucleotides in Figure 4C). Analysis of the TOB^{5+}-induced midpoints (Figure 4C, left panel) for these transitions reveals that tRNA^{Asp} unfolds in two distinct transitions. The first unfolding transition ($TOB_{1/2} = 0.12 \pm 0.01$ mM) is detected as strong increases in reactivity at U59 and U60 in the T-loop (solid symbols, Figure 4B). U60 stacks on U59 which then stacks on A15 in the D-loop. These nucleotides thus comprise a part of the tertiary interactions that link the D- and T-loops. Smaller magnitude reactivity increases also occur at positions A57 and A58 in this loop (open symbols, Figure 4B). A58 participates in a *cis*-U−A base pair involving the Watson–Crick and Hoogsteen faces of these two bases (left panel, Figure 4C). Given that TOB^{5+}-induced disruption of tRNA^{Asp} structure is first detected at the adjacent U59 and U60 positions and at the cross-loop U54−A58 pair, these data suggest that the primary binding site for TOB^{5+} is in the T-loop. T-loop sequences in tRNA^{Asp} differ from those in tRNA^{Phe} and these differences may explain the ability of TOB^{5+} to selectively bind tRNA^{Asp} in preference to tRNA^{Phe} (*16*).

All other nucleotides participate in the second transition ($TOB_{1/2} = 0.51 \pm 0.17$ mM). TOB^{5+} induces wholesale unfolding of the D-stem, coupled with disruption of almost all of the remaining tertiary interactions as evidenced by significant increases in SHAPE reactivity throughout these structures (second panel, Figure 4B). We also observe reproducible decreases in SHAPE reactivity at nucleotides G37 and C38 (third panel, Figure 4B) and we speculate that these nucleotides may be constrained by TOB^{5+} binding in the anticodon loop. These experiments emphasize, first, that TOB^{5+} interacts in selective way in the T-loop and, second, that Mg^{2+} and TOB^{5+} modulate tRNA^{Asp} folding in idiosyncratic ways.

DISCUSSION

The results of diverse studies focusing on different RNAs emphasize that RNA molecules populate numerous intermediate and alternate states as they fold (*1, 3, 25–30*). RNA thus traverses an energy landscape that contains a fleeting unfolded state, a complex set of intermediate states, and finally, the native state

$$\text{unfolded} \rightleftharpoons [\text{intermediates}] \rightleftharpoons \text{native}$$

In-depth and accurate information for these intermediate states is essential to understand the barriers in RNA folding reactions, the interactions of ions and other ligands with RNA, and the roles that proteins play in supporting and modulating RNA folding reactions. Intermediate states are likely to be complex mixtures of conformations with similar energies. It is thus very difficult to obtain definitive structural information for most intermediate states. In lieu of sufficiently detailed information, intermediate states are often modeled as having roughly the same secondary structure as the final native state but to lack native tertiary interactions. Less frequently, specific alternative base pairing interactions have been identified for some intermediate states. Ideally, analysis of the energetic and structural contributions of intermediates in RNA folding reactions requires a detailed accounting of all nucleotide interactions in these states.

The properties of intermediate states are influenced by many factors, including the three perturbants whose effect has now been assessed for tRNA^{Asp} transcripts (this work and ref *17*): Mg^{2+}, small molecule binding, and temperature. SHAPE chemistry allows the effects of perturbations to be monitored at single nucleotide resolution at almost every position in an RNA (Figures 3A and 4A). Strikingly, we find that each of these denaturation methods causes the RNA to unfold by a different pathway (Figure 5). Transitions observed for tRNA^{Asp} transcripts often involve just one or two nucleotides and could have been easily missed using less comprehensive approaches for analyzing RNA structure.

In the case of the removal of Mg^{2+} (Figure 5, left), SHAPE data are consistent with a one-step rearrangement from the native state to a structure containing an extended duplex involving the D- and anticodon stems. Once Mg^{2+} no longer stabilizes tertiary interactions, stable G−C pairs are favored over the less stable pairs that form in the native structure. Thus, Mg^{2+} sequesters nucleotides in tertiary interactions as it stabilizes the native structure at the expense of alternate structures and base pairings.

Perturbing the structure of tRNA^{Asp} by thermal denaturation (*17*) also results in complex unfolding steps, involving an energetically linked loss of tertiary and secondary structure, followed by a conformational shift (right panels, Figure 5). The data are consistent with a significant rearrangement in base pairing which, similar to the effect of removing Mg^{2+}, is inconsistent with the common assumption that intermediate states can be adequately characterized as a loose, but nativelike, secondary structure.

TOB^{5+} induces a subtler two-step, unfolding transition (Figure 5, bottom). The first involves disruption of the T- and D-loop interactions. Further addition of TOB^{5+} causes

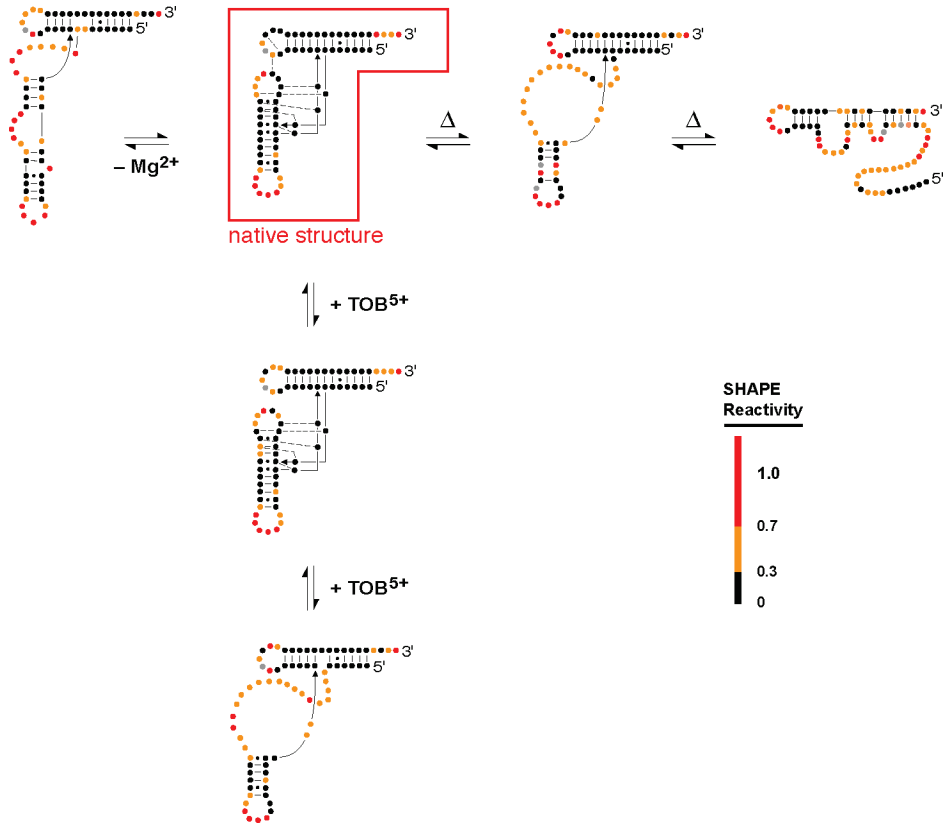

FIGURE 5: Complex structural transitions for $tRNA^{Asp}$ transcripts. Left, unfolding induced by removal of Mg^{2+}; right, temperature-induced unfolding (Δ); bottom, structural consequences of TOB^{5+} binding. Transitions are unique to each denaturant. Nucleotides are shown as circles and are colored by their absolute SHAPE reactivities. For simplicity, only a subset of the temperature-dependent transitions (*17*) is shown.

complete loss of base paring in the D-stem. Counterintuitively, structural destabilization of the native $tRNA^{Asp}$ fold by TOB^{5+} is more similar to the intermediates obtained upon thermal denaturation than to the state obtained by titrating Mg^{2+} (compare first structure shown for thermal denaturation with the final TOB^{5+}-induced structure, Figure 5).

Interrogation of $tRNA^{Asp}$ transcript structure reveals that unanticipatedly diverse sets of intermediates are accessible from the native state. A significant subset of these unfolding reactions involves either linked loss of base pairing and tertiary interactions or significant shifts in base pairing (Figure 5). For the specific example of $tRNA^{Asp}$, these states are therefore inconsistent with the view that RNA folding is hierarchical or that RNA folding intermediates can be well-characterized as having near-native secondary structures. SHAPE chemistry offers a robust approach for developing newly detailed understandings of the energetic contributions of intermediate states in this and many other RNA folding reactions.

EXPERIMENTAL PROCEDURES

RNA. The $tRNA^{Asp}$ transcript was synthesized by in vitro transcription in the context of a structure cassette containing 5′ and 3′ flanking sequences that facilitate analysis of the internal sequences by primer extension, as described (*21*). The RNA was purified by denaturing electrophoresis, eluted from the gel, and stored in 10 mM Hepes (pH 8.0) and 1 mM EDTA.

Ligand-Dependent RNA Structure Analysis. RNA [4 pmol; in 6 or 5 μL of 5 mM Hepes (pH 8.0) for the Mg^{2+}- and TOB^{5+}-dependent experiments, respectively] was heated at 95 °C for 2 min, cooled on ice for 2 min, treated with 3 μL of 3.3 × folding buffer [333 mM NaCl, 333 mM HEPES (pH 8.0), $MgCl_2$], and incubated at 37 °C for 15 min. For the Mg^{2+}-dependent experiments, final [$MgCl_2$] concentrations spanned 0–20 mM (20, 15, 11, 8.0, 6.0, 5.0, 3.5, 2.5, 2.0, 1.5, 1.2, 0.90, 0.65, 0.50, 0.25, 0.20, 0.15, 0.10, and 0 mM; in Figure 3). For the TOB^{5+} experiments, the [$MgCl_2$] was 6 mM and TOB^{5+} (1 μL) was added to the refolded RNA to a final concentration of 0.01–6 mM (0, 0.010, 0.014, 0.020, 0.025, 0.030, 0.040, 0.060, 0.080, 0.10, 0.15, 0.20, 0.25, 0.35, 0.45, 0.60, 0.80, 1.0, 1.4, 1.9, 2.5, 3.5, 4.5, and 6.0 mM; in Figure 4). The RNA was treated with 1M7 (*22*) (1 μL, 30 mM in anhydrous DMSO), allowed to react for five reagent hydrolysis half-lives (70 s), and placed on ice. Control reactions contained 1μL of DMSO in lieu of 1M7. Modified RNAs were recovered by precipitation with ethanol and sites of 2′-*O*-adduct formation were detected by reverse transcriptase-mediated primer extension (*21, 31*).

Analysis of Ligand-Induced Transitions. Primer extension reactions were resolved on sequencing gels and the gel image was quantified by phosphorimaging. Individual band intensities were integrated using SAFA (*32*). After subtracting background, lane-to-lane variations in nucleotide reactivity were normalized by the sum of the total intensities for the 75 $tRNA^{Asp}$ nucleotides. Data obtained as a function of ligand concentrations were rescaled to a unit (0 to 1) scale and smoothed using a rolling weighting function (*17, 33*). Transition midpoints ($Mg_{1/2}$ and $TOB_{1/2}$) were obtained by fitting individual band intensities (I) to the equation, $I = A[L]/([L] + L_{1/2}) + b$, where [L] is the ligand concentration,

$L_{1/2}$ is the transition midpoint, *A* is the transition amplitude, and *b* is a (small) baseline offset. To report absolute SHAPE reactivities for a single state (as shown in Figure 5), individual band intensities were normalized to a scale that spans 0 to ~1.5. SHAPE reactivities were divided by the average of the 10% of the most highly reactive positions, after excluding the most reactive 2% of intensities. By this calculation, the average intensity of highly reactive positions is defined as 1.0.

Error Analysis. All experiments were repeated at least twice, but typically 3–5 times. For an experiment repeated independently under a single set of conditions (like the native, $-Mg^{2+}$, and $+TOB^{5+}$structures shown in Figure 2), the standard deviation in absolute SHAPE reactivity at any given position is typically 0.03–0.07 SHAPE units. Standard deviations at individual position for the titration experiments (Figures 3 and 4) performed in parallel were ±0.05 SHAPE units.

RNA Structural Models. RNA structural models for the unfolded states of $tRNA^{Asp}$ that form in the absence of Mg^{2+} or the presence of TOB^{5+} were developed using a thermodynamic folding algorithm as implemented in the RNAstructure program (*34*). SHAPE reactivities were used to constrain the output of the predicted secondary structures as quasi-energetic constraints (ref *35* and unpublished results).

REFERENCES

1. Cole, P. E., Yang, S. K., and Crothers, D. M. (1972) Conformational changes of transfer ribonucleic acid. Equilibrium phase diagrams. *Biochemistry 11*, 4358–4368.
2. Tinoco, I., and Bustamante, C. (1999) How RNA folds. *J. Mol. Biol. 293*, 271–281.
3. Buchmueller, K. L., Webb, A. E., Richardson, D. A., and Weeks, K. M. (2000) A collapsed, non-native RNA folding state. *Nat. Struct. Biol. 7*, 362–366.
4. Draper, D. E., Grilley, D., and Soto, A. M. (2005) Ions and RNA folding. *Annu. Rev. Biophys. Biomol. Struct. 34*, 221–243.
5. Woodson, S. A. (2005) Metal ions and RNA folding: a highly charged topic with a dynamic future. *Curr. Opin. Chem. Biol. 9*, 104–109.
6. Romani, A. M., and Scarpa, A. (2000) Regulation of cellular magnesium. *Front. Biosci. 5*, D720–D734.
7. Manning, G. S. (1978) The molecular theory of polyelectrolyte solutions with applications to the electrostatic properties of polynucleotides. *Q. Rev. Biophys. 11*, 179–246.
8. Draper, D. E. (2004) A guide to ions and RNA structure. *RNA 10*, 335–343.
9. Misra, V. K., and Draper, D. E. (2000) Mg^{2+} binding to tRNA revisited: the nonlinear Poisson-Boltzmann model. *J. Mol. Biol. 299*, 813–825.
10. Walter, F., Vicens, Q., and Westhof, E. (1999) Aminoglycoside-RNA interactions. *Curr. Opin. Chem. Biol. 3*, 694–704.
11. Jin, E., Katritch, V., Olson, W. K., Kharatisvili, M., Abagyan, R., and Pilch, D. S. (2000) Aminoglycoside binding in the major groove of duplex RNA: the thermodynamic and electrostatic forces that govern recognition. *J. Mol. Biol. 298*, 95–110.
12. Kaul, M., and Pilch, D. S. (2002) Thermodynamics of aminoglycoside-rRNA recognition: the binding of neomycin-class aminoglycosides to the A site of 16S rRNA. *Biochemistry 41*, 7695–7706.
13. Yang, G., Trylska, J., Tor, Y., and McCammon, J. A. (2006) Binding of aminoglycosidic antibiotics to the oligonucleotide A-site model and 30S ribosomal subunit: Poisson-Boltzmann model, thermal denaturation, and fluorescence studies. *J. Med. Chem. 49*, 5478–5490.
14. Kirk, S. R., and Tor, Y. 1999) tRNA(Phe) binds aminoglycoside antibiotics. *Bioorg. Med. Chem. 7*, 1979–1991.
15. Mikkelsen, N. E., Johansson, K., Virtanen, A., and Kirsebom, L. A. (2001) Aminoglycoside binding displaces a divalent metal ion in a tRNA-neomycin B complex. *Nat. Struct. Biol. 8*, 510–514.
16. Walter, F., Pütz, J., Giegé, R., and Westhof, E. (2002) Binding of tobramycin leads to conformational changes in yeast tRNA(Asp) and inhibition of aminoacylation. *EMBO J. 21*, 760–768.
17. Wilkinson, K. A., Merino, E. J., and Weeks, K. M. (2005) RNA SHAPE chemistry reveals non-hierarchical interactions dominate equilibrium structural transitions in $tRNA^{Asp}$ transcripts. *J. Am. Chem. Soc. 127*, 4659–4667.
18. Badorrek, C. S., and Weeks, K. M. (2005) RNA flexibility in the dimerization domain of a gamma retrovirus. *Nature Chem. Biol. 1*, 104–111.
19. Badorrek, C. S., and Weeks, K. M. (2006) Architecture of a gamma retroviral genomic RNA dimer. *Biochemistry 45*, 12664–12672.
20. Gherghe, C., and Weeks, K. M. (2006) The SL1-SL2 (stem-loop) domain is the primary determinant for stability of the gamma retroviral genomic RNA dimer. *J. Biol. Chem. 281*, 37952–37961.
21. Merino, E. J., Wilkinson, K. A., Coughlan, J. L., and Weeks, K. M. (2005) RNA Structure Analysis at Single Nucleotide Resolution by Selective 2′-Hydroxyl Acylation and Primer Extension (SHAPE). *J. Am. Chem. Soc. 127*, 4223–4231.
22. Mortimer, S. A., and Weeks, K. M. (2007) A fast-acting reagent for accurate analysis of RNA secondary and tertiary structure by SHAPE chemistry. *J. Am. Chem. Soc. 129*, 4144–4145.
23. Perret, V., Garcia, A., Grosjean, H., Ebel, J.-P., Florentz, C., and Giegé, R. (1990) Relaxation of a transfer RNA specificity by removal of modified nucleotides. *Nature 344*, 787–789.
24. Chamberlin, S. I., and Weeks, K. M. (2000) Mapping local nucleotide flexibility by selective acylation of 2′-amine substituted RNA. *J. Am. Chem. Soc. 122*, 216–224.
25. Crothers, D. M., Cole, P. E., Hilbers, C. W., and Shulman, R. G. (1974) The molecular mechanism of thermal unfolding of Escherichia coli formylmethionine transfer RNA. *J. Mol. Biol. 87*, 63–88.
26. Celander, D. W., and Cech, T. R. (1991) Visualizing the higher order folding of a catalytic RNA molecule. *Science 251*, 401–407.
27. Gluick, T. C., and Draper, D. E. (1994) Thermodynamics of folding a pseudoknotted mRNA fragment. *J. Mol. Biol. 241*, 246–262.
28. Wu, M., and Tinoco, I. (1998) RNA folding causes secondary structure rearrangement. *Proc. Natl. Acad. Sci. U.S.A. 95*, 11555–11560.
29. Buchmueller, K. L., and Weeks, K. M. (2003) Near native structure in an RNA collapsed state. *Biochemistry 42*, 13869–13878.
30. Fang, X. W., Thiyagarajan, P., Sosnick, T. R., and Pan, T. (2002) The rate-limiting step in the folding of a large ribozyme without kinetic traps. *Proc. Natl. Acad. Sci. U.S.A. 99*, 8518–8523.
31. Wilkinson, K. A., Merino, E. J., and Weeks, K. M. (2006) Selective 2′-Hydroxyl Acylation analyzed by Primer Extension (SHAPE): Quantitative RNA structure analysis at single nucleotide resolution. *Nature Protocols 1*, 1610–1616.
32. Das, R., Laederach, A., Pearlman, S. M., Herschlag, D., and Altman, R. B. (2005) SAFA: Semi-automated footprinting analysis software for high-throughput quantification of nucleic acid footprinting experiments. *RNA 11*, 344–354.
33. Chambers, J. M., Cleveland, W. S., Kleiner, B., and Tukey, P. A. (1983) *Graphical Methods for Data Analysis*, pp 91–104, Wadsworth International Group, Belmont, CA.
34. Mathews, D., Disney, M., Childs, J., Schroeder, S., Zuker, M., and Turner, D. (2004) Incorporating chemical modification constraints into a dynamic programming algorithm for prediction of RNA secondary structure. *Proc. Natl. Acad. Sci. U.S.A. 101*, 7287–7292.
35. Wilkinson, K. A., Gorelick, R. J., Vasa, S. M., Guex, N., Rein, A., Mathews, D. H., Giddings, M. C., and Weeks, K. M. (2008) High-throughput SHAPE analysis reveals structures in HIV-1 genomic RNA strongly conserved across distinct biological states. *PLoS Biol.*, in press.
36. Westhof, E., Dumas, P., and Moras, D. (1985) Crystallographic refinement of yeast aspartic acid transfer RNA. *J. Mol. Biol. 184*, 119–145.
37. Westhof, E., Dumas, P., and Moras, D. (1988) Restrained refinement of two crystalline forms of yeast aspartic acid and phenylalanine transfer RNA crystals. *Acta Crystallogr., Sect. A 44*, 112–123.
38. Chin, K., Sharp, K. A., Honig, B., and Pyle, A. M. (1999) Calculating the electrostatic properties of RNA provides new insights into molecular interactions and function. *Nat. Struct. Biol. 6*, 1055–1061.
39. Baker, N. A., Sept, D., Joseph, S., Holst, M. J., and McCammon, J. A. (2001) Electrostatics of nanosystems: application to microtubules and the ribosome. *Proc. Natl. Acad. Sci. U.S.A. 98*, 10037–10041.

BI702372X